THE JOURNAL OF BIOLOGICAL CHEMISTRY VOL. 285, NO. 37, pp. 28674–28682, September 10, 2010

Neuroligin Trafficking Deficiencies Arising from Mutations in the α/β-Hydrolase Fold Protein Family*

Received for publication, May 5, 2010, and in revised form, July 6, 2010 Published, JBC Papers in Press, July 8, 2010, DOI 10.1074/jbc.M110.139519

Antonella De Jaco[‡§¶], Michael Z. Lin[‖1], Noga Dubi[‡], Davide Comoletti[‡], Meghan T. Miller[‡], Shelley Camp[‡], Mark Ellisman[**], Margaret T. Butko[‖], Roger Y. Tsien[‖], and Palmer Taylor[‡2]

From the [‡]Department of Pharmacology, Skaggs School of Pharmacy and Pharmaceutical Sciences, the [‖]Departments of Pharmacology and Chemistry and Biochemistry, and the [**]Department of Neuroscience, University of California, San Diego, La Jolla, California 92093 and the [§]Department of Cell and Developmental Biology, "Daniel Bovet" Neurobiology Research Center, and the [¶]Istituto Pasteur-Fondazione Cenci Bolognetti, Sapienza University of Rome, 00185 Rome, Italy

Despite great functional diversity, characterization of the α/β-hydrolase fold proteins that encompass a superfamily of hydrolases, heterophilic adhesion proteins, and chaperone domains reveals a common structural motif. By incorporating the R451C mutation found in neuroligin (NLGN) and associated with autism and the thyroglobulin G2320R (G221R in NLGN) mutation responsible for congenital hypothyroidism into NLGN3, we show that mutations in the α/β-hydrolase fold domain influence folding and biosynthetic processing of neuroligin3 as determined by *in vitro* susceptibility to proteases, glycosylation processing, turnover, and processing rates. We also show altered interactions of the mutant proteins with chaperones in the endoplasmic reticulum and arrest of transport along the secretory pathway with diversion to the proteasome. Time-controlled expression of a fluorescently tagged neuroligin in hippocampal neurons shows that these mutations compromise neuronal trafficking of the protein, with the R451C mutation reducing and the G221R mutation virtually abolishing the export of NLGN3 from the soma to the dendritic spines. Although the R451C mutation causes a local folding defect, the G221R mutation appears responsible for more global misfolding of the protein, reflecting their sequence positions in the structure of the protein. Our results suggest that disease-related mutations in the α/β-hydrolase fold domain share common trafficking deficiencies yet lead to discrete congenital disorders of differing severity in the endocrine and nervous systems.

The neuroligins (NLGNs)[3] are postsynaptic proteins that associate with cognate presynaptic partners, the neurexins (1–3, α and β) (NRXNs) (1, 2), and are essential for selectivity in synaptic function (3). By virtue of a common structure in their extracellular domain, the NLGNs fall in the α/β-hydrolase fold superfamily of proteins. To date, proteins of this family are known to serve three general functions: 1) catalyzing the hydrolysis of ester and amide substrates as with acetylcholinesterase, 2) serving as chaperones for secretion of hormone precursors such as with thyroglobulin (Tg), and 3) mediating heterophilic synaptic adhesion interactions as found for neuroligin. The common structure of the α/β-hydrolase fold domain shared by the family members (4) suggests that despite the different functions, these proteins share common mechanisms of protein folding and processing.

In NLGN, the α/β-hydrolase fold domain is crucial for transsynaptic interactions with NRXN. Both the NRXNs and the NLGNs are transmembrane proteins; they facilitate associations with intracellular proteins at synaptic loci in pre- and postsynaptic neurons (5). Genetic aberrations in both the NLGN and the NRXN protein families have been identified in patients with autism spectrum disorders (6–13). The R451C substitution in the α/β-hydrolase fold domain of NLGN3 was found in two autistic brothers (7), and this mutation has been characterized extensively. Protein derived from R451C NLGN3 cDNA is predominantly retained in the endoplasmic reticulum (ER) when transfected into HEK293, COS, and hippocampal neurons (14–17). Moreover construction of knock-in mice confirmed *in vivo* the effect of this amino acid change (18). Three-dimensional structures of NLGN4 and the NLGN1-NRXN1-β complex (19–21) reveal that R451C maps to a position remote from the binding site for NRXN1-β (21), suggesting that this mutation likely impairs protein folding and processing rather than disrupting the binding domain.

Mutations in the α/β-hydrolase fold domain of Tg are commonly found in association with congenital hypothyroidism, causing arrest of intracellular processing and secretory transport (22). The mutation G2320R in Tg maps in the α/β-hydrolase fold domain of the protein and is responsible for congenital non-goitrous hypothyroidism and dwarfism (23, 24). The Tg G2320R mutant protein is retained within the ER with persistent cysteine thiol exposure consistent with thiol-mediated ER retention (25).

By incorporating the R451C and G221R (G2320R in Tg) mutations into NLGN3, we show that mutations in the α/β-hydrolase fold domain strikingly influence folding and biosynthetic processing of NLGN3. Although the undifferentiated HEK293 cells show how the mutations affect the global processing of the α/β-hydrolase fold proteins, transfection of

* This work was supported, in whole or in part, by National Institutes of Health Grants P42 ES010337 and R37 GM-18360 from the United States Public Health Service (to P. T.). This work was also supported by a grant from the Compagnia San Paolo Bando Programma in Neuroscienze 2008 (to A. D. J.) and Autism Speaks Grant 2617 (to D. C.).

[1] Present address: Departments of Pediatrics and Bioengineering, Stanford University, Stanford, CA 94305.

[2] To whom correspondence should be addressed: Tel.: 858-534-4028; Fax: 858-534-8248; E-mail: pwtaylor@ucsd.edu.

[3] The abbreviations used are: NLGN, neuroligin; NRXN, neurexins; Tg, thyroglobulin; ER, endoplasmic reticulum; Endo H, endoglycosidase H; PNGase F, *N*-glycosidase F; HCV, hepatitis C virus; PDI, protein-disulfide isomerase.

genes encoding the mutant protein into neurons enables us to examine processing and transport to synapses in the context of the specialized cell type. Moreover, we demonstrate that the compromise of trafficking and export correlates with the degree of misfolding caused by each mutation.

EXPERIMENTAL PROCEDURES

Construction of Neuroligin Expression Plasmids—FLAG-tagged cDNAs encoding rat WT NLGN3 and the mutant R451C were described previously (16, 26). G221R and truncation (stop codon inserted at Tyr-640) were introduced in rat NLGN3 full-length constructs by site-directed mutagenesis using the QuikChange mutagenesis kit (Stratagene, San Diego, CA), verified by restriction digests and DNA sequencing and subsequently subcloned back into the original NLGN3 vector. Large scale plasmid purifications used DEAE columns (Qiagen Inc., Valencia, CA).

Cell Culture and DNA Transfections—HEK293 cells were maintained at 37 °C, 10% CO_2 in Dulbecco's modified Eagle's medium (DMEM) containing 10% fetal bovine serum and 2 mM L-glutamine. NLGN cDNA constructs were transfected into HEK293 cells using FuGENE 6 (Roche Applied Science) both for transient expression studies and to establish stably transfected cell lines, which were selected with 800 μg/ml G418 (Geneticin, Sigma-Aldrich) as described previously (27).

Immunocytochemistry for Confocal Microscopy—Parental HEK293, WT NLGN3, or G221R NLGN3 stably expressing cells were plated on poly-D-lysine-coated glass coverslips and grown in DMEM. Cells were fixed in 4% paraformaldehyde in phosphate-buffered saline (PBS), washed, and labeled for immunofluorescence (16) using an anti-FLAG M2 monoclonal antibody (1:500) (Sigma) and an anti-calreticulin polyclonal antibody (1:200) (Assay Design/StressGen, Ann Arbor, MI) in blocking buffer diluted 5-fold (PBS, 2% normal donkey serum, 0.5% BSA, and 50 mM glycine). FITC-conjugated anti-rabbit and Cy5-conjugated anti-mouse secondary antibodies (Jackson ImmunoResearch, West Grove, PA) were diluted 1:100 in the same buffer. Image processing employed a MRC-1024 laser-scanning confocal system (Bio-Rad) coupled to a Zeiss Axiovert 35 M microscope.

Immunoprecipitation—HEK293 cells stably expressing NLGN3 WT or R451C or G221R mutant proteins were washed twice in PBS, and harvested in lysis buffer (140 mM NaCl, 3 mM $MgCl_2$, 10 mM Tris-HCl, pH 8, 0.5% Nonidet P-40, and 5 μg/ml leupeptin). After a 30-min incubation on ice, nuclear and cellular debris were removed by centrifugation at 14,000 *g* at 4 °C for 10 min. Cell lysate total protein (~500 μg) was incubated with 4.8 μg of anti-FLAG antibody in 0.5 ml for 2 h, and 30 μl of immobilized protein G (Thermo Fisher Scientific) was then added for 1.5 h. Beads were then washed three times with T-TBS (20 mM Tris-HCl, pH 7.6, 137 mM NaCl, 0.2% Tween), and proteins were eluted by boiling in 30 μl of 2× SDS sample buffer (100 mM Tris-HCl, pH 6.8, 4% SDS, 2% β-mercaptoethanol, 0.2% bromphenol blue, and 20% glycerol). Samples were spun briefly to remove the beads. Proteins in the supernatant were collected for Western blot analysis. For large scale protein purification to analyze chaperone content, cells were washed, harvested with PBS, and extracted with lysis buffer containing 10 mM *N*-ethylmaleimide (Pierce). After protein immunoprecipitation using an anti-FLAG antibody, immunocomplexes were washed in 150 mM NaCl, 10 mM HEPES, pH 7. NLGN proteins were eluted with FLAG peptide (500 μg/ml) in 50 mM glycine, pH 2.

Western Blots and Immunoblotting—Western blots were performed using standard techniques including 10% SDS-polyacrylamide gels (Invitrogen) and Immobilon P membranes (Millipore, Bedford, MA). The commercial anti-neuroligin mouse monoclonal (clone 4F9, catalog number 129 011 Synaptic Systems, Goettingen, Germany) was used for NLGN detection (see Figs. 2*B*, 3, and 4) at a dilution of 1:1000. Dilutions and sources of primary antibodies used for chaperone detection (see Figs. 2*A* and 3) are as follows: anti-calreticulin rabbit polyclonal antibody, 1:2000; anti-calnexin rabbit polyclonal antibody, 1:2000; anti-HSP70 rabbit polyclonal antibody, 1:30,000; anti-PDI rabbit polyclonal antibody, and 1:4000 (all from Assay Design/StressGen); anti-GRP78 (GRP78/BiP) rabbit polyclonal antibody, 1 μg/ml; anti-GRP94 rabbit polyclonal antibody, 1:2000; anti-ERp57 rabbit polyclonal antibody, 1:2000; anti-HSP90 rabbit polyclonal antibody, 1 μg/ml; anti-PDIr rabbit polyclonal antibody, 1:1000; anti-ERp72 rabbit polyclonal antibody, and 5 μg/ml (all from Abcam, Cambridge, MA).

Endoglycosidase H and N-Glycosidase F Digestions—Immunoprecipitated proteins were boiled for 10 min in commercial glycoprotein denaturing buffer and digested with endoglycosidase H (Endo H) in G5 Reaction Buffer at 37 °C for 3 h (New England Biolabs, Beverly, MA). Alternatively, proteins were treated with *N*-glycosidase F (PNGase F) in G7 Reaction Buffer (New England Biolabs) for 1 h at 37 °C. Digests were subjected to SDS-PAGE and immunoblotted using the anti-NLGN commercial antibody described above.

Proteolytic Digests—NLGN3 proteins from HEK293 cells stably transfected with WT or mutant constructs were immunoprecipitated and treated with trypsin (specific activity: 10,000 units/mg of protein) (Sigma-Aldrich) in 50 mM Tris-HCl, pH 7.4. Beads containing the immunoprecipitated NLGN protein were incubated at room temperature for the times indicated in Fig. 4. Trypsin concentration used for WT and the R451C mutant protein was 3 μg/ml, and for the G221R protein, trypsin concentration was 1 μg/ml. The reaction was stopped by heating the samples at 90 °C after the addition of SDS-PAGE loading buffer. Protein degradation was analyzed by SDS-PAGE and immunoblotting using the commercial anti-NLGN antibody.

Metabolic Labeling and Immunoprecipitation—HEK293 cells stably expressing WT or mutant NLGN3 proteins were grown in methionine- and cysteine-free DMEM (Invitrogen) for 30 min at 37 °C and then pulsed for 30 min with 0.5 mCi/ml [^{35}S]methionine and [^{35}S]cysteine (PerkinElmer Life Sciences) at 37 °C. The labeled amino acids were then chased for intervals of 0.5–48 h by incubating the cells in DMEM containing 5% FBS and 5 mM unlabeled methionine and cysteine (Sigma-Aldrich). At the end of the chase, cells were harvested, and proteins were solubilized in lysis buffer and immunoprecipitated using an anti-FLAG antibody (Sigma-Aldrich) and immobilized protein G for 3 h. Beads were washed four times with 0.1% Tween 20 in Tris-buffered saline (TBS), and proteins were eluted by adding SDS-PAGE loading buffer and heating for 5

min at 90 °C. The proteins were separated on a 10% SDS-PAGE gel, and the gel was then incubated for 30 min in a fixing solution (1% acetic acid, 25% isopropyl alcohol in water) followed by a 30-min incubation in amplifying solution (GE Healthcare). The gel was dried, and the radioactive signal was visualized by fluorography.

TimeSTAMP2-YFP—pcDNA3 plasmids expressing NLGN3 WT, G221R, or R451C were fused at the C terminus to an improved TimeSTAMP[4] cassette containing Venus yellow fluorescent protein with an internal hepatitis C virus (HCV) protease site and the sequence for HCV protease (TimeSTAMP2-YFP).[5] In this reporter, the *cis*-HCV protease inactivates the Venus FP, producing a non-fluorescent protein. Fluorescent protein can be obtained by adding the specific HCV protease inhibitor, BILN-2061 (28). Postnatal day 1 rat hippocampal neurons were co-transfected, immediately after dissection and dissociation, with an NLGN expression plasmid and an mOrange plasmid to monitor transfection efficiency, using the Amaxa Nucleofection system for neurons (Lonza, Walkersville, MD) according to the manufacturer's protocol. Neurons were then plated on poly-D-lysine-coated glass-bottomed imaging dishes and cultured in Neurobasal-A media with B27 (Invitrogen) for 2 weeks, refreshing half the culture medium twice weekly. At 10–12 days, neurons were imaged on an inverted confocal fluorescence microscope in a humidified chamber at 35 °C in Hanks' balanced salt solution supplemented with B27, 5.5 mM glucose, 1 mM pyruvate, and 10 mM HEPES, pH 7.3. 5 μM BILN-2061 was added during the pulse period and removed by three washes before the chase period. For assessing the role of proteasome-mediated degradation, the proteasome inhibitor MG132 (5 μM) (Sigma-Aldrich) was applied to one set of cells during the chase. Imaging was performed with a 40× oil objective and illuminated with a 75-watt Xenon arc lamp via a 10% neutral density filter. At each time point, six optical sections of yellow fluorescent protein (YFP) fluorescence (excitation filter 495/10 nm, emission filter 535/25 nm, exposure time 1 s) and mOrange2 fluorescence (excitation filter 540/25 nm, emission filter 595/50 nm, exposure time 100 ms) spaced 2 μm apart were obtained through the entire thickness of multiple mOrange-expressing neurons. Image analysis was performed on maximum intensity projections in a blinded fashion using the program ImageJ. Mean fluorescence intensity was obtained from regions of interest drawn over the brightest continuous perinuclear region (to quantify ER-Golgi protein) and over a 30-μm segment of dendrite 30 μm away from the soma (to quantify dendritic protein) by hand. Fluorescence from background regions of untransfected cells was subtracted before ratio calculation.

RESULTS

The NLGN3 G221R Mutation Results in ER Retention—A comparison of the sequences encoding proteins of the α/β-hydrolase fold family reveals that amino acid Gly-2320 in Tg is conserved at homologous positions in NLGN, acetylcholinesterase, and butyrylcholinesterase in several animal species, suggesting that this residue is critical in the assembly of the tertiary structure of the protein family members (Fig. 1*A*). In addition, structural data indicate that this residue is positioned in the core of the α/β-hydrolase fold domain of NLGN, and substitution to arginine, a bulky cationic amino acid, is likely to perturb the overall structure of the protein (Fig. 1*B*) (21). We chose to use NLGN3 as a model protein to compare the influence of this mutation on biosynthesis and processing of the gene product in parallel with the previously characterized R451C mutation.

Through co-localization studies with the ER marker calreticulin, we observed that NLGN3 G221R is retained in the ER instead of migrating to the cell surface as seen with the WT protein (Fig. 2*A*). Further evidence that the NLGN3 G221R mutant protein is retained in the ER is shown by the analysis of glycosylation. Fig. 2*B* (*left panel*) shows that both WT and mutant G221R NLGN3 cDNAs, truncated at Tyr-640 just before a cluster of *O*-linked glycosylation signals, produce the expression of proteins of similar mass that are completely sensitive to PNGase F, a glycosidase that cleaves between the innermost GlcNAc and the asparagine residue of *N*-linked oligosaccharides and is not sensitive to terminal oligosaccharide processing. Conversely, the full-length NLGN3 protein shows a significant mass difference between the fully *N*- and *O*-glycosylated WT protein and the G221R mutant whose biosynthesis has been arrested in the ER and is therefore not *O*-glycosylated. Treatment with PNGase F (Fig. 2*B*, *middle panel*) shows that the size difference between WT and mutant proteins is maintained when *N*-linked sugars are removed (due to the presence of *O*-linked sugars on the WT protein that are absent in the immature ER-retained G221R NLGN3). Treatment with Endo H, an enzyme that preferentially digests high mannose immature oligosaccharides (found on the proteins in transit in the ER) rather than the mature, processed *N*-glycans on the WT protein, confirms the ER localization of the G221R mutant protein. The mutant protein is susceptible to Endo H, whereas no deglycosylation shift is observed with the WT protein. These results establish that NLGN3 G221R is retained in the ER, as observed for G2320R Tg in the thyrocytes of *rdw* rats (23), whereas WT NLGN3 undergoes *N*- and *O*-linked glycosylation in the Golgi (Fig. 2*B*, *right panel*).

G221R and R451C Mutations Alter Chaperone Interactions—To identify ER chaperones that assist in the folding of native NLGN3 and to analyze differential association between chaperones that associate with WT and mutant proteins, we immunoprecipitated NLGN3 from stably expressing HEK293 cells and then immunoblotted to identify specific ER chaperone proteins. We show that GRP78/BiP and GRP94 associate more avidly with R451C and G221R mutant proteins than the WT protein (Fig. 3), whereas the lectins, calnexin and calreticulin, show an association with both WT and mutant proteins.

Because NLGN3 presents both disulfide bonds and free cysteines, we tested interaction with oxidoreductases belonging to the PDI family and found that PDIr, ERp57, and ERp72 are associated with the mutant proteins, but not with WT NLGN3. PDI is the only member of the family that shows a specific interaction with the G221R mutant protein; it does not stably associate with WT or R451C NLGN3. Cytosolic molecular chaperones show differential behavior; HSP90 interacts only with the mutant proteins, whereas HSP70 associates strongly

[4] TimeSTAMP is a time-specific tagging for the age measurement of proteins.
[5] M. Z. Lin, J. Yang, M. T. Butko, and R. Y. Tsien, manuscript in preparation.

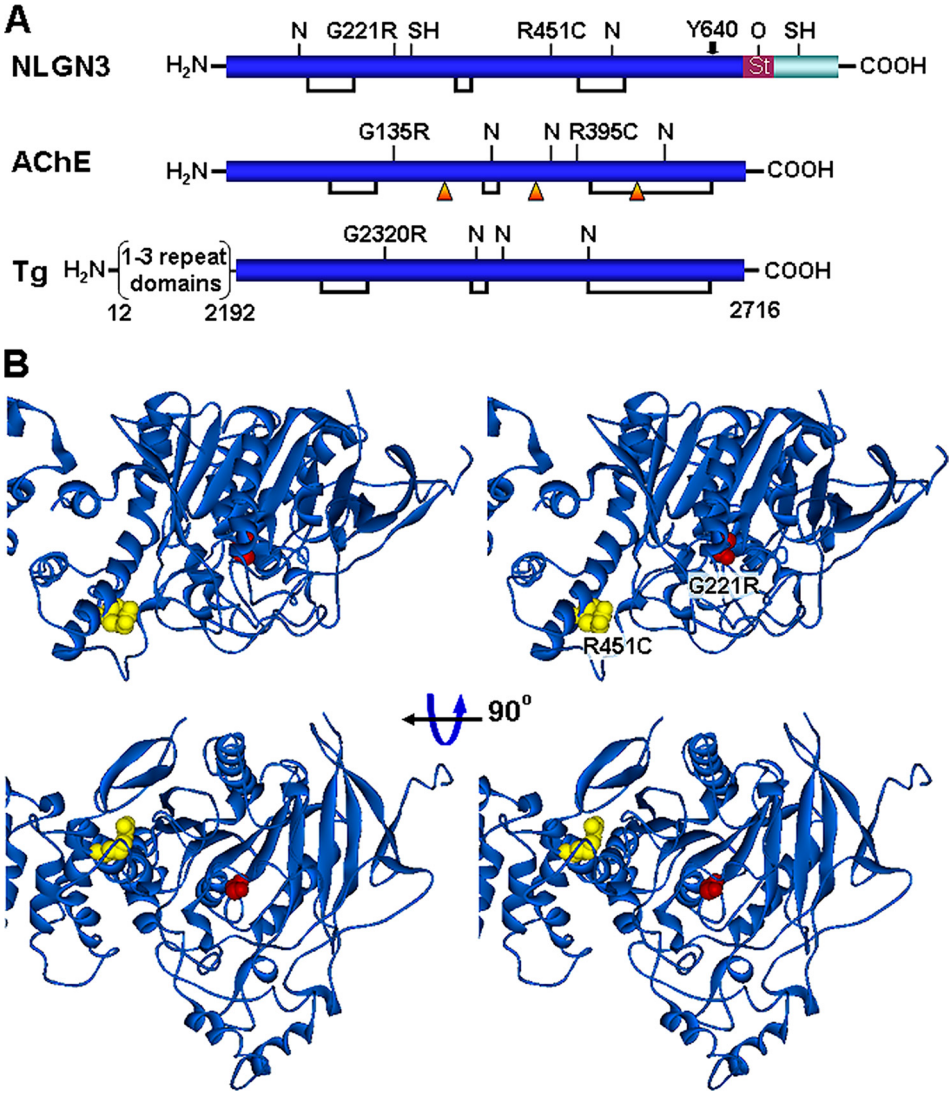

FIGURE 1. **Schematic representation of mutations studied in NLGN3.** *A*, the diagram of NLGN3 shows G221R (found in Tg) and R451C (found in NLGN3) mutations. Shown below are the corresponding mutations at the homologous positions in acetylcholinesterase (*AchE*) and thyroglobulin. Positions of *N*-linked glycosylation sites (*N*) (Asn-98 and Asn-522 in NLGN3) are shown on top of the α,β-hydrolase fold domain (*blue bar*). Disulfide bonds (*rectangular shapes*) and unpaired cysteines (at positions 293 and 775 in NLGN3) are shown. *St* indicates the stalk domain (*pink*), the site of *O*-linked glycosylation (*O*). Amino acid numbering of NLGN3 is according to Ref. 1. NLGN3 was truncated at position Tyr-640 (*arrow*) to produce a soluble protein. *Orange arrowheads* show the acetylcholinesterase catalytic triad. *B*, stereo view of the NLGN4 structure. The homologous NLGN4 crystal structure is used to show the following mutations: G221R (*red*) and R451C (*yellow*). Note that Gly-221 is buried in the core of the acetylcholinesterase domain and that Arg-451 is near the surface of the protein.

with the WT protein. These data indicate that the folding of native NLGN3 nascent protein recruits several chaperone proteins and also that retention of the mutant nascent proteins in the ER results from association with different classes of ER resident chaperones.

Association of ER chaperones with WT and mutant NLGN3 proteins was also investigated using mass spectrometry analysis. In agreement with the immunoblots (Fig. 3), data collection showed that Grp78/BiP is the most abundant ER chaperone found associated with both R451C and G221R mutant proteins, but not with the WT protein.[6]

[6] A. De Jaco and M. Ghassemian, unpublished data.

Proteolytic Digests Reveal Different Degrees of Misfolding in NLGN3 Mutants—We used limited trypsin proteolysis (29) to probe the potential misfolding of R451C and G221R NLGN3. Equal amounts of WT and mutant proteins were purified by immunoprecipitation from cell extracts of stably transfected HEK293 cells and exposed to trypsin for varying incubation times at room temperature (Fig. 4). At a trypsin concentration of 3 μg/ml, the extent of protein degradation of the R451C mutant protein was analyzed over 60 min (Fig. 4*B*). For the G221R mutant protein, nearly complete degradation was evident within 30 min at 1 μg/ml (Fig. 4*A*). In comparison, WT NLGN3 showed no degradation using these digestion conditions (Fig. 4, *A* and *B*). Parallel incubations in the absence of trypsin show no protein degradation for the mutant proteins. The protease sensitivity of R451C NLGN3 suggests that this mutation results in the protein assuming a locally expanded and flexible conformation conferring exposure of trypsin-sensitive sites. G221R NLGN3 shows even greater sensitivity to trypsin than R451C, suggesting that the bulky, charged arginine side chain in the core of the α/β-hydrolase fold domain greatly affects overall protein folding, perhaps producing a molten globule state (30).

R451C and G221R Mutations Differentially Influence Processing Rates—We performed metabolic labeling experiments in HEK293 cells expressing the NLGN3 proteins to monitor rates of protein maturation and degradation (Fig. 5). Following a 30-min pulse with ^{35}S-labeled amino acids and variable chase intervals with unlabeled amino acids, we observed that processing of the WT protein is complete in less than 3 h, as indicated by the appearance of the slower migrating species (Fig. 5*A*, *top panel*) in SDS gels. At 6 h, the WT NLGN3 protein reaches a maximal protein expression level with a slow decay that decreases to the level of minimal detection in ~48 h. The presence of the R451C mutation greatly diminishes the processing of NLGN3 (Fig. 5*A*, *middle panel*). In fact, after a 3-h chase, the mutant protein remains substantially unprocessed, with only a small fraction appearing in a band corresponding to the fully processed WT protein. This fraction appears to increase over 6 h and disappears at a slightly faster

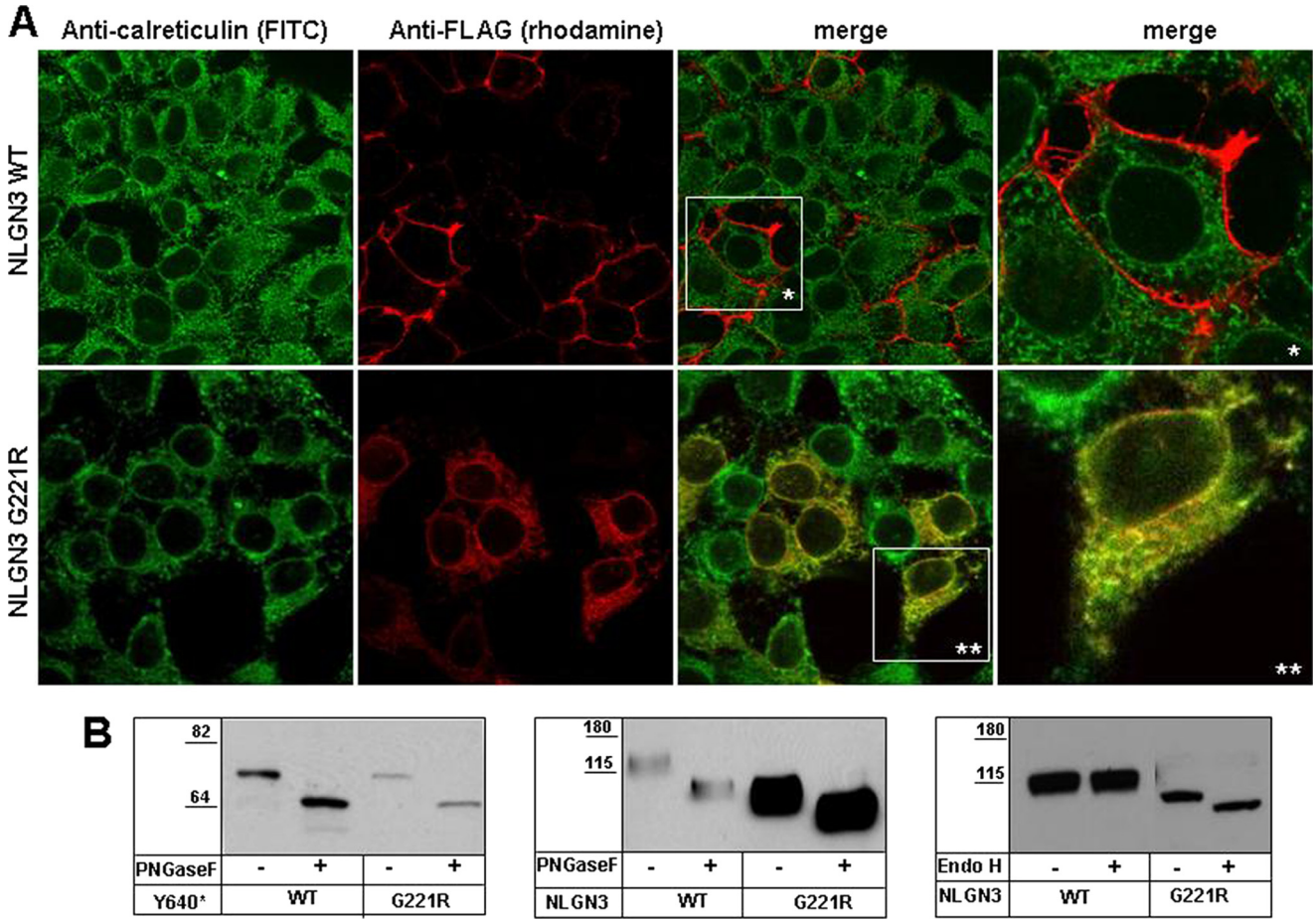

FIGURE 2. **Cellular trafficking of WT and G221R NLGN3.** *A*, representative immunofluorescent images of HEK293 cells expressing FLAG-tagged NLGN3 full-length proteins (*upper panels*, WT; *lower panels*, G221R mutation). Images show co-localization staining for the ER marker calreticulin (*green*), the NLGN3-FLAG tag (*red*), and the merged view of the two signals, which reveals a *yellow color* that represents co-localized proteins. A magnification of the merged panel is shown for NLGN3 WT (*) and G221R (**). *B*, glycosidase treatment of truncated and full-length immunoprecipitated NLGN3 proteins, WT, and G221R. *Left panel*, PNGase F treatment of NLGN3 soluble proteins. NLGN3 is truncated at position Tyr-640. *Middle panel*, PNGase F treatment of full-length NLGN3 proteins. *Right panel*, NLGN3 proteins incubated with Endo H. All digests are followed by SDS-PAGE and immunoblotting using an anti-NLGN antibody. Molecular mass markers are shown in kDa. Both mutant and WT proteins, whether or not the *O*-glycosylated tether and membrane span are deleted, show more rapid migration following PNGase F cleavage of the *N*-linked oligosaccharides, whereas only the G221R mutant protein is subject to digestion by the high mannose directed glycosidase, Endo H.

rate than the WT protein. A lower molecular mass band, likely a degradation product, accumulates over ~24 h.

Even more dramatic differences are observed when processing of the G221R protein is analyzed (Fig. 5*A*, *lower panel*). Virtually all the G221R mutant protein remains unprocessed and is degraded more rapidly than the R451C protein. However, due to the high sensitivity of the pulse-chase technique when compared with the steady-state immunofluorescence and Western blot approaches (Fig. 2), we do see a very low concentration of the mature G221R protein that becomes evident over the initial 1.5 h. When the metabolic labeling is conducted in the presence of proteasome inhibitors, either lactacystin or MG123 (Fig. 5*B*), the fractional increase in expression of the G221R protein after a 3-h chase is substantially higher than that of the WT protein, indicating that the mutant protein is preferentially degraded via the proteasome pathway. These data indicate a substantial difference in the turnover rate of WT and mutant proteins and suggest that the preferential degradation pathway for the G221R NLGN3 mutant involves the proteasome.

Trafficking of WT, R451C, and G221R NLGN3 in Single Hippocampal Neurons—To examine the influence of mutations in NLGN3 on the trafficking in the cellular context of the nervous system, we transfected WT and mutant NLGN3 proteins fused to a novel fluorescent reporter into isolated hippocampal neurons that are able to form synaptic connections in culture. The fluorescent reporter tag, TimeSTAMP2-YFP, consists of a *cis*-acting protease from the HCV and YFP with an internal HCV cleavage site. Newly synthesized tagged proteins are not fluorescent because the YFP is cleaved in-*cis* by the HCV. The addition of BILN-2061 rescues YFP fluorescence by virtue of its inhibition of HCV; the tagged protein (WT or mutant NLGN3) after BILN-2061 addition is fluorescent (28). Time-lapse microscopy with this reporter allows visualization of newly synthesized NLGN3 proteins as they traffic to their final destination.

We co-transfected postnatal day 1 rat hippocampal neurons with NLGN3 fused to the TimeSTAMP2-YFP tag (NLGN3-TimeSTAMP2-YFP) and the orange fluorescent protein, mOrange2 (as a marker for transfection), and allowed the

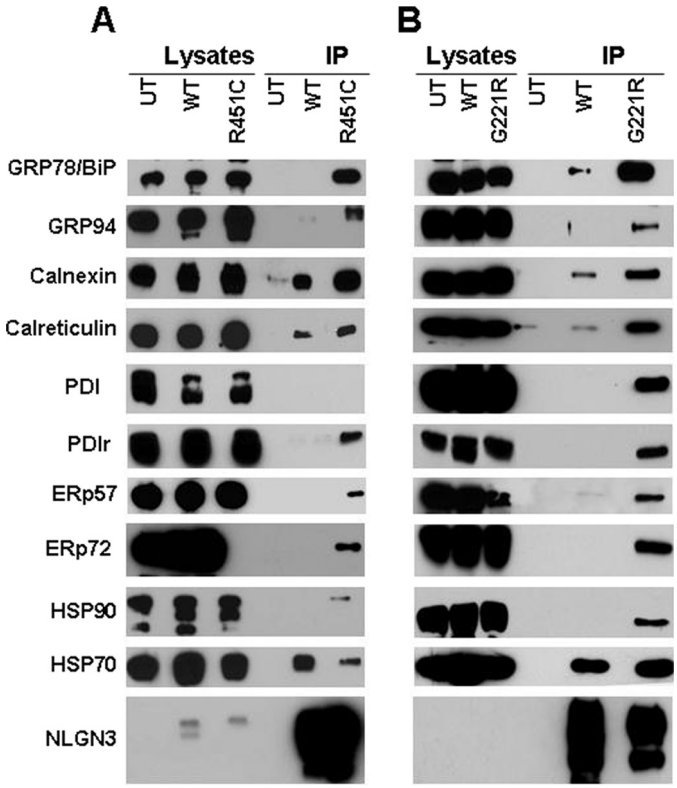

FIGURE 3. **Association of ER chaperones with WT, R451C, and G221R NLGN3.** Full-length proteins were immunoprecipitated from lysates of stably transfected HEK293 cells with anti-FLAG antibody. Lysates and immunoprecipitated purified samples were immunoblotted using available commercial antibodies for multiple chaperone proteins. An anti-NLGN antibody was used to detect immunoprecipitated NLGN3 as a control. ER chaperones show more association with the R451C and G221R mutant NLGN3 proteins than with the WT protein. In particular, the chaperone PDI appears to associate selectively with the G221R mutant protein. *UT*, untransfected cells; *IP*, immunoprecipitated protein. *A*, WT and R451C NLGN3. *B*, WT and G221R NLGN3.

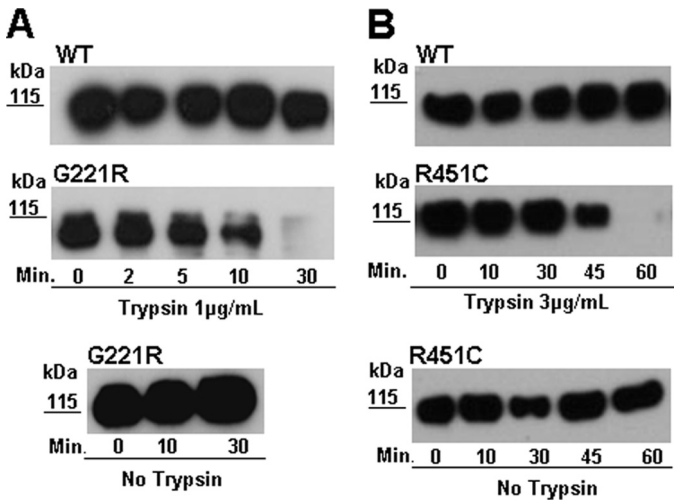

FIGURE 4. **Protease sensitivity of WT and mutant NLGN3 proteins.** WT, R451C, and G221R NLGN3 proteins were digested with trypsin and analyzed by reducing SDS-PAGE followed by immunoblotting with an anti-NLGN antibody. *Upper panels* show trypsin digests of WT and mutant proteins. *Lower panels* show incubations of mutant proteins in the absence of trypsin. Mutant proteins are more sensitive to trypsin than the WT protein. *A*, WT and G221R NLGN3. *B*, WT and R451C NLGN3.

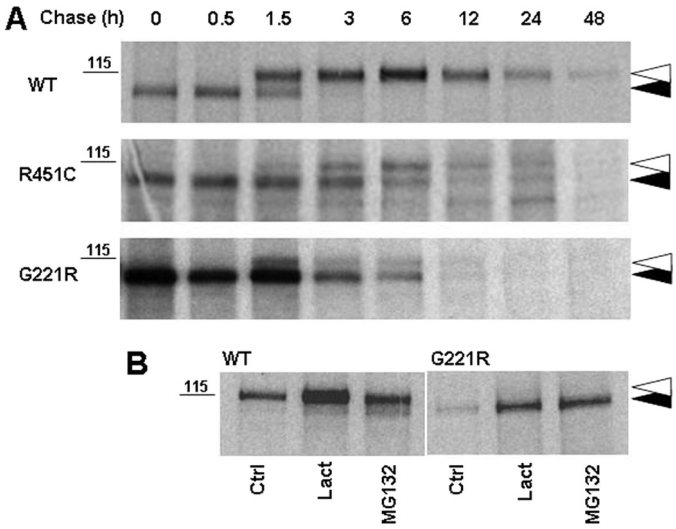

FIGURE 5. **Intracellular processing of WT, R451C, and G221R NLGN3 proteins.** HEK293 cells stably transfected with WT, R451C, or G221R NLGN3 cDNAs were pulse-labeled with [^{35}S]methionine and [^{35}S]cysteine. The labeling was followed by incubation with unlabeled amino acids for the times indicated. Labeled NLGN3 proteins were immunoprecipitated from cell lysates with anti-FLAG antibody and analyzed by SDS-PAGE. *A*, biosynthesis and processing from 0 to 48 h after labeling are shown for WT, R451C, and G221R NLGN3 proteins. Unprocessed (*filled arrowheads*) and fully processed (*open arrowheads*) proteins are marked. The two mutant proteins show retarded glycosylation processing when compared with the WT over the first 6 h and more rapid rates of turnover of the nascent protein. *B*, processing of WT and G221R NLGN3 proteins in the absence (*Ctrl*) or the presence of 5 μM proteasome inhibitors, lactacystin (*Lact*), or MG132. A single time point, 3 h after labeling, is shown.

neurons to differentiate over 2 weeks. Without exposure to the protease inhibitor BILN-2061, neurons show only red-orange fluorescence (Fig. 6*A*, *left column*). We then added 5 μM BILN-2061 and visualized newly synthesized protein over the next 18 h. Fluorescence in the ER-Golgi regions and in the dendrites (beyond 30 μm from the cell body) was quantified at 18 h and compared for WT, R451C, and G221R versions of NLGN3-TimeSTAMP2-YFP (Fig. 6*B*). NLGN3 G221R shows minimal export to dendrites, whereas NLGN3 R451C is exported at levels intermediate between WT and G221R (Fig. 6*B*, $n = 13$ each, $p < 10^{-6}$ by analysis of variance, $p < 0.03$ between groups by pairwise t test). Visualizing new protein localization revealed that WT NLGN3-TimeSTAMP2-YFP is efficiently inserted into synapses, as shown by punctate green staining in the neurons in Fig. 6*A* (*top row*). The R451C mutation in NLGN3 causes a reduction in the export of the protein to dendritic locations when compared with the WT protein (Fig. 6*A*, *middle row*). Neurons that expressed R451C at higher levels revealed that some mutated protein was trafficked to the dendrites, but with very low efficiency (Fig. 6*A*, *middle row*, *right column*).

The most impaired trafficking is observed with the NLGN3 G221R protein. In this case, we find minimal protein in the axon trunk and dendritic shaft with virtually no localization to dendritic synapses, even in strongly expressing neurons (Fig. 6*A*, *bottom row*). These results in neurons are in accord with our observations in HEK293 cells where the G221R and R451C mutations hinder protein processing, with the G221R mutation causing the most severe defect.

To understand the influence of the above mutations on processing rates, we performed time-lapse imaging at times extend-

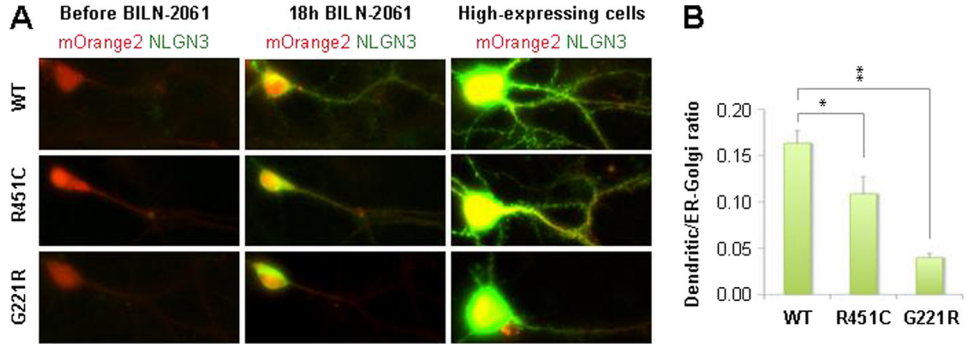

FIGURE 6. **Trafficking of NLGN3 in rat hippocampal neurons.** *A*, representative images of newly synthesized NLGN3 in hippocampal neurons using the TimeSTAMP2-YFP labeling technique are shown. Neurons from postnatal day 0 rats were transfected and cultured for 14 days, and data were collected 18 h after the administration of BILN-2061. A gradient of newly synthesized NLGN3 (*green*) from the soma to the dendrites is observed for the WT protein after 18 h. R451C and G221R mutant proteins show a defect in the translocation of the proteins through the axon trunk into the dendrites. mOrange2 (*red*) is a marker of transfection. The *left column* shows cells before BILN-2061 administration. The *middle column* shows cells 18 h after BILN-2061 administration. The *right column* shows a greater magnification of high expressing cells. *B*, quantitative analysis of protein translocation from the ER-Golgi compartment to the dendrites 18 h after BILN-2061 administration. Thirteen cells from each NLGN transfection, WT, R451C, or G221R were analyzed; the dendritic/ER-Golgi ratios of WT were significantly different from those of the mutants. *, $p = 0.023$, **, $p < 0.000001$, analysis of variance $p < 0.000001$. *Bars* represent S.E.

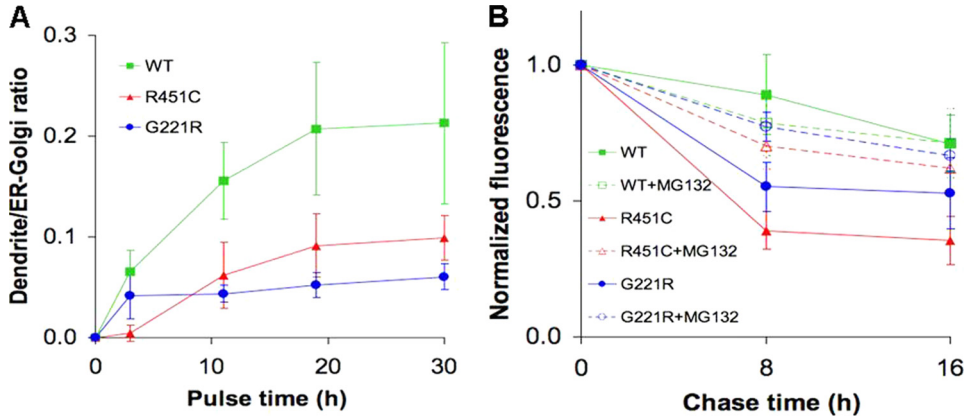

FIGURE 7. **Processing and degradation rates of NLGN3 in rat hippocampal neurons.** *A*, quantification of the export of WT, R451C, and G221R NLGN3 at different times. The ratio of fluorescent NLGNs in the dendrites to those in the ER-Golgi region is quantified over time. *B*, degradation of fluorescent WT, R451C, and G221R NLGNs in the ER-Golgi region over time is shown in the presence and absence of the proteasome inhibitor MG132. Initial fluorescence is arbitrarily set to 1.0. *Bars* represent S.E.

ing to 30 h (Fig. 7*A*). Analysis of ER-Golgi and dendritic fluorescence showed that steady-state distributions are approached by 18 h. R451C slowed protein progression through the secretory pathway relative to WT (Fig. 7*A*). Note that there is a complete absence of dendritic protein at 3 h with R451C, whereas with WT NLGN3, progression is about one-third complete. The G221R mutation even more dramatically reduced the amount of protein exiting the soma (Fig. 7*A*). Interestingly, a small amount of G221R protein is exported to dendrites and appears without much delay; this small increase correlates with an initial spike in our metabolic pulse-chase results (Fig. 5, *A* and *B*).

Enhanced Proteasome Clearance of NLGN3 Mutant Proteins—After removal of BILN-2061, the fluorescence that has developed on TimeSTAMP2-YFP-labeled proteins remains stable, thereby providing a means to visualize protein turnover of newly synthesized proteins that were fluorescently labeled during BILN-2061 administration.[4] By quantifying fluorescence in the ER-Golgi region at various times during the chase period after BILN-2061 removal, we were able to estimate rates of degradation of proteins within the secretory pathway. Both R451C and G221R mutants are cleared from the ER-Golgi at faster rates than WT (Fig. 7*B*). Most of this difference is attributable to enhanced protein cleared in the proteasome as it is largely rescued by treatment with MG132 during the chase period (Fig. 7*B*). These results confirm that the NLGN3 mutants are susceptible to proteasome-mediated degradation during processing in the neuronal secretory pathway.

DISCUSSION

Proteins belonging to the α/β-hydrolase fold superfamily are thought to have diverged from a common ancestral gene (31). Although different in function and oligomeric assemblies, NLGNs, cholinesterases, and Tg share a common α/β-hydrolase fold domain that plays a critical structural role for heterophilic adhesion, hydrolase catalysis, and hormone secretion, respectively (4, 32). Rare mutations affecting *NLGN*4 and *NLGN*3 genes have been found in patients with autistic traits (33, 34) Most of the mutations map to the α/β-hydrolase fold domain of the NLGNs, mainly causing loss of function of the affected protein (35). The region homologous to the cholinesterases in Tg represents only 20% of the entire encoded open reading frame. This domain facilitates trafficking and secretion of the protein that is ultimately processed to the thyroid hormones (36). The α/β-hydrolase fold domain of Tg is rich in natural mutations that have been linked to primary congenital hypothyroidism and are characterized by ER retention and subsequent thyroid hormone deficiency (22, 37, 38).

We show that the G221R mutation causes ER retention of NLGN3 in a manner that is similar to what is seen with the homologous Tg G2320R mutation in *rdw*/*rdw* rats (23, 24), most likely due to the structural role of the glycine residue in the α/β-hydrolase fold domain of both proteins. Processing of the G221R mutation is compared with the R451C natural substitution found in NLGN3 that has been characterized by our group as well as others, which shows incomplete ER retention of the mutant protein (14–18). We present direct evidence that the G221R and R451C mutations cause different degrees of misfolding of the α/β-hydrolase fold domain in NLGN3, highlighting the importance of the correct folding of this domain for transport of the protein from the ER to

the correct final cellular location as it has been previously proposed for Tg (39).

By using a biochemical imaging approach, we demonstrate that the R451C mutation reduces the rate of maturation of NLGN3 and its transport through the dendrites to reach the synapses, whereas the G221R mutation nearly completely blocks protein maturation, showing that the rank order of protein trafficking defects analyzed in HEK293 cells are conserved in hippocampal neurons. Our data support the concept that G221R is responsible for global misfolding due to its position in the core of the α/β-hydrolase fold domain, whereas the R451C substitution is responsible for local misfolding, consistent with its location on the surface of the protein (Fig. 2*B*) (21). That multiple chaperones and oxidoreductases interact with misfolded mutant NLGN3 proteins is consistent with blockade of trafficking steps in the ER. Increased chaperone association with the mutant protein when compared with WT NLGN3 indicates that ER quality control blocks R451C and G221R misfolded proteins from exiting the ER, potentially assisting them in achieving the correct folding status (40). There is an obvious chaperone association observed between the mutant proteins and the ER stress chaperone GRP78/BiP, suggesting that misfolding might activate signal transduction pathways that orchestrate the unfolded protein response (41, 42).

Investigation of protein interactions with members of the PDI family has resulted in a particularly interesting finding; PDI selectively associates with NLGN3 G221R, but not with R451C and WT proteins. This can be explained in light of the multifunctional role of PDI as an oxidoreductase (in the formation and isomerization of disulfide bonds) and a chaperone (40, 43) and its recently proposed function in accelerating ER-associated degradation (44). PDI association with G221R might reflect activation of a cellular response to global misfolding, not seen in the response to a localized perturbation. Because PDI family members present different roles in promoting protein maturation by catalyzing specific reactions (45), interactions of NLGN3 with other members of the family have been investigated. Both G221R and R451C mutant proteins associate with PDIr, ERp57, and ERp72, suggesting the activation of a thiol-mediated ER retention mechanism for mutant NLGN3 proteins. At the same time, the association of Erp57 with the mutant proteins is not surprising because NLGN3 is glycosylated and is a partner for calnexin and calreticulin as shown by the co-immunoprecipitation data. Association between NLGN3 and the cytosolic chaperones HSP90 and HSP70 has also been tested. Exclusive interaction of HSP90 with the mutant proteins might show a role in promoting degradation through the proteasome as shown previously for the cystic fibrosis transmembrane conductance regulator (46).

Recently, NLGN3-deficient mice have been reported as displaying a behavioral phenotype that resembles symptoms typical of autism spectrum disorders (47). At the same time, mice expressing the NLGN3 R451C mutation not only show reduced socialization behavior but also present an increased frequency of inhibitory synaptic events, leading the investigators to propose that the R451C mutation exerts its effects through a gain-of-function mechanism (18). A gain of function of NLGN3 would be unlikely if protein maturation and export were completely blocked by the mutation. Our data support the proposal that the R451C protein does retain the capacity for interacting with intracellular partners such as PSD-95 and likely sequesters them into malfunctioning or destabilized complexes, supporting the hypothesis that behavioral changes can be linked to a subtle perturbation of synaptic functions.

Dissecting the molecular mechanisms that alter protein folding of NLGN3 offers new insights into designing pharmacological approaches that could allow the rescue of impaired trafficking of the α/β-hydrolase fold domain proteins. Moreover, such studies could be useful for observing the effects of environmental toxicants to which trafficking of these synaptic and hormone secretory proteins might be sensitized.

Here we describe the use of a novel imaging tool, TimeSTAMP2-YFP, that offers the advantage of quantitatively monitoring the distribution of newly synthesized NLGN3 at the level of a single neuron. Moreover, screening of future mutations arising in the α/β-hydrolase fold domain should help to identify congenital disorders with neurological and endocrine consequences such as autism spectrum disorders for the NLGNs, hypothyroidism for Tg, and prolonged succinyl apnea for butyrylcholinesterase (17, 48).

Acknowledgments—We thank Majid Ghassemian and Elizabeth Komives, Department of Chemistry and Biochemistry, University of California, San Diego for mass spectrometry analysis.

REFERENCES

1. Ichtchenko, K., Nguyen, T., and Südhof, T. C. (1996) *J. Biol. Chem.* **271,** 2676–2682
2. Song, J. Y., Ichtchenko, K., Südhof, T. C., and Brose, N. (1999) *Proc. Natl. Acad. Sci. U.S.A.* **96,** 1100–1105
3. Chubykin, A. A., Atasoy, D., Etherton, M. R., Brose, N., Kavalali, E. T., Gibson, J. R., and Südhof, T. C. (2007) *Neuron* **54,** 919–931
4. Ollis, D. L., Cheah, E., Cygler, M., Dijkstra, B., Frolow, F., Franken, S. M., Harel, M., Remington, S. J., Silman, I., Schrag, J., *et al*. (1992) *Protein Eng.* **5,** 197–211
5. Scholl, F. G., and Scheiffele, P. (2003) *Trends Neurosci.* **26,** 618–624
6. Feng, J., Schroer, R., Yan, J., Song, W., Yang, C., Bockholt, A., Cook, E. H., Jr., Skinner, C., Schwartz, C. E., and Sommer, S. S. (2006) *Neurosci. Lett.* **409,** 10–13
7. Jamain, S., Quach, H., Betancur, C., Råstam, M., Colineaux, C., Gillberg, I. C., Soderstrom, H., Giros, B., Leboyer, M., Gillberg, C., and Bourgeron, T. (2003) *Nat. Genet.* **34,** 27–29
8. Laumonnier, F., Bonnet-Brilhault, F., Gomot, M., Blanc, R., David, A., Moizard, M. P., Raynaud, M., Ronce, N., Lemonnier, E., Calvas, P., Laudier, B., Chelly, J., Fryns, J. P., Ropers, H. H., Hamel, B. C., Andres, C., Barthélémy, C., Moraine, C., and Briault, S. (2004) *Am. J. Hum. Genet.* **74,** 552–557
9. Lawson-Yuen, A., Saldivar, J. S., Sommer, S., and Picker, J. (2008) *Eur. J. Hum. Genet.* **16,** 614–618
10. Talebizadeh, Z., Lam, D. Y., Theodoro, M. F., Bittel, D. C., Lushington, G. H., and Butler, M. G. (2006) *J. Med. Genet.* **43,** e21
11. Yan, J., Noltner, K., Feng, J., Li, W., Schroer, R., Skinner, C., Zeng, W., Schwartz, C. E., and Sommer, S. S. (2008) *Neurosci. Lett.* **438,** 368–370
12. Yan, J., Oliveira, G., Coutinho, A., Yang, C., Feng, J., Katz, C., Sram, J., Bockholt, A., Jones, I. R., Craddock, N., Cook, E. H., Jr., Vicente, A., and Sommer, S. S. (2005) *Mol. Psychiatry* **10,** 329–332
13. Zhang, C., Milunsky, J. M., Newton, S., Ko, J., Zhao, G., Maher, T. A., Tager-Flusberg, H., Bolliger, M. F., Carter, A. S., Boucard, A. A., Powell, C. M., and Südhof, T. C. (2009) *J. Neurosci.* **29,** 10843–10854
14. Chih, B., Afridi, S. K., Clark, L., and Scheiffele, P. (2004) *Hum. Mol. Genet.*

13, 1471–1477
15. Chubykin, A. A., Liu, X., Comoletti, D., Tsigelny, I., Taylor, P., and Südhof, T. C. (2005) *J. Biol. Chem.* **280,** 22365–22374
16. Comoletti, D., De Jaco, A., Jennings, L. L., Flynn, R. E., Gaietta, G., Tsigelny, I., Ellisman, M. H., and Taylor, P. (2004) *J. Neurosci.* **24,** 4889–4893
17. De Jaco, A., Comoletti, D., Kovarik, Z., Gaietta, G., Radic, Z., Lockridge, O., Ellisman, M. H., and Taylor, P. (2006) *J. Biol. Chem.* **281,** 9667–9676
18. Tabuchi, K., Blundell, J., Etherton, M. R., Hammer, R. E., Liu, X., Powell, C. M., and Südhof, T. C. (2007) *Science* **318,** 71–76
19. Araç, D., Boucard, A. A., Ozkan, E., Strop, P., Newell, E., Südhof, T. C., and Brunger, A. T. (2007) *Neuron* **56,** 992–1003
20. Chen, X., Liu, H., Shim, A. H., Focia, P. J., and He, X. (2008) *Nat. Struct. Mol. Biol.* **15,** 50–56
21. Fabrichny, I. P., Leone, P., Sulzenbacher, G., Comoletti, D., Miller, M. T., Taylor, P., Bourne, Y., and Marchot, P. (2007) *Neuron* **56,** 979–991
22. Vono-Toniolo, J., Rivolta, C. M., Targovnik, H. M., Medeiros-Neto, G., and Kopp, P. (2005) *Thyroid* **15,** 1021–1033
23. Hishinuma, A., Furudate, S., Oh-Ishi, M., Nagakubo, N., Namatame, T., and Ieiri, T. (2000) *Endocrinology* **141,** 4050–4055
24. Kim, P. S., Ding, M., Menon, S., Jung, C. G., Cheng, J. M., Miyamoto, T., Li, B., Furudate, S., and Agui, T. (2000) *Mol. Endocrinol.* **14,** 1944–1953
25. Menon, S., Lee, J., Abplanalp, W. A., Yoo, S. E., Agui, T., Furudate, S., Kim, P. S., and Arvan, P. (2007) *J. Biol. Chem.* **282,** 6183–6191
26. Comoletti, D., Flynn, R. E., Boucard, A. A., Demeler, B., Schirf, V., Shi, J., Jennings, L. L., Newlin, H. R., Südhof, T. C., and Taylor, P. (2006) *Biochemistry* **45,** 12816–12827
27. Comoletti, D., Flynn, R., Jennings, L. L., Chubykin, A., Matsumura, T., Hasegawa, H., Südhof, T. C., and Taylor, P. (2003) *J. Biol. Chem.* **278,** 50497–50505
28. Lin, M. Z., Glenn, J. S., and Tsien, R. Y. (2008) *Proc. Natl. Acad. Sci. U.S.A.* **105,** 7744–7749
29. Gong, Q., Jones, M. A., and Zhou, Z. (2006) *J. Biol. Chem.* **281,** 4069–4074
30. Dolginova, E. A., Roth, E., Silman, I., and Weiner, L. M. (1992) *Biochemistry* **31,** 12248–12254
31. Cousin, X., Hotelier, T., Giles, K., Lievin, P., Toutant, J. P., and Chatonnet, A. (1997) *Nucleic Acids Res.* **25,** 143–146
32. Carr, P. D., and Ollis, D. L. (2009) *Protein Pept Lett.* **16,** 1137–1148
33. Bourgeron, T., Leboyer, M., and Delorme, R. (2009) *Bull. Acad. Natl. Med.* **193,** 299–305
34. Südhof, T. C. (2008) *Nature* **455,** 903–911
35. Lintas, C., and Persico, A. M. (2009) *J. Med. Genet.* **46,** 1–8
36. Caron, P., Moya, C. M., Malet, D., Gutnisky, V. J., Chabardes, B., Rivolta, C. M., and Targovnik, H. M. (2003) *J. Clin. Endocrinol. Metab.* **88,** 3546–3553
37. Caputo, M., Rivolta, C. M., Esperante, S. A., Gruñeiro-Papendieck, L., Chiesa, A., Pellizas, C. G., González-Sarmiento, R., and Targovnik, H. M. (2007) *Clin. Endocrinol. (Oxf.)* **67,** 351–357
38. Pardo, V., Rubio, I. G., Knobel, M., Aguiar-Oliveira, M. H., Santos, M. M., Gomes, S. A., Oliveira, C. R., Targovnik, H. M., and Medeiros-Neto, G. (2008) *Thyroid* **18,** 783–786
39. Lee, J., Di Jeso, B., and Arvan, P. (2008) *J. Clin. Invest.* **118,** 2950–2958
40. Hebert, D. N., and Molinari, M. (2007) *Physiol. Rev.* **87,** 1377–1408
41. Bertolotti, A., Zhang, Y., Hendershot, L. M., Harding, H. P., and Ron, D. (2000) *Nat. Cell Biol.* **2,** 326–332
42. Kaufman, R. J. (2002) *J. Clin. Invest.* **110,** 1389–1398
43. Wilkinson, B., and Gilbert, H. F. (2004) *Biochim. Biophys. Acta* **1699,** 35–44
44. Forster, M. L., Sivick, K., Park, Y. N., Arvan, P., Lencer, W. I., and Tsai, B. (2006) *J. Cell Biol.* **173,** 853–859
45. Ellgaard, L., and Ruddock, L. W. (2005) *EMBO Rep.* **6,** 28–32
46. Loo, M. A., Jensen, T. J., Cui, L., Hou, Y., Chang, X. B., and Riordan, J. R. (1998) *EMBO J.* **17,** 6879–6887
47. Radyushkin, K., Hammerschmidt, K., Boretius, S., Varoqueaux, F., El-Kordi, A., Ronnenberg, A., Winter, D., Frahm, J., Fischer, J., Brose, N., and Ehrenreich, H. (2009) *Genes Brain Behav.* **8,** 416–425
48. Yen, T., Nightingale, B. N., Burns, J. C., Sullivan, D. R., and Stewart, P. M. (2003) *Clin. Chem.* **49,** 1297–1308